# RheoTack—An approach to investigate retraction rate dependent detaching behavior of pressure sensitive adhesives

Michael Meurer,[1,2] Tim Prescher,[1] Esther Ramakers-van Dorp,[1] Bernhard Möginger,[1] and Berenika Hausnerova[2,3,a)]

[1]*Department of Natural Sciences, University of Applied Sciences Bonn-Rhein-Sieg, Von-Liebig-Str. 20, D-53359 Rheinbach, Germany*
[2]*Department of Production Engineering, Faculty of Technology, Tomas Bata University in Zlin, Vavreckova 275, 76001 Zlín, Czech Republic*
[3]*Centre of Polymer Systems, Institute Tomas Bata University in Zlín, 76001 Zlín, Czech Republic*

(Received 29 November 2021; final revision received 21 February 2022; published 21 March 2022)

**Abstract**

Characterization methods of pressure sensitive adhesives (PSA) originate from technical bonding and do not cover relevant data for the development and quality assurance of medical applications, where PSA with flexible backing layers are adopted to human skin. In this study, a new method called RheoTack is developed to determine (mechanically and optically) an adhesion and detaching behavior of flexible and transparent PSA based patches. Transdermal therapeutic systems (TTS) consisting of silicone-based PSAs on a flexible and transparent backing layer were tested on a rotational rheometer with an 8 mm plate as a probe rod at retraction speeds of 0.01, 0.1, and 1 mm/s with respect to their adhesion and detaching behavior in terms of force-retraction displacement curves. The curves consist of a compression phase to affirm wetting; a tensile deformation phase intercepting stretching, cavity, and fibril formation; and a failure phase with detaching. Their analysis provides values for stiffness, force, and displacement of the beginning of fibril formation, force and displacement of the beginning of a failure due to fibril breakage and detaching, as well as corresponding activation energies. All these parameters exhibit the pronounced dependency on the retraction speed. The force-retraction displacement curves together with the simultaneous video recordings of the TTS deformation from three different angles (three cameras) provide deeper insight into the deformation processes and allow for interpreting the properties' characteristics for PSA applications.  https://doi.org/10.1122/8.0000405

## I. INTRODUCTION

Transdermal therapeutic systems (TTS) represent an example of elaborate medical patches consisting of pressure sensitive adhesives (PSA) containing active pharmaceutical substances and a flexible backing layer. PSA are adhesives that are applied to substrates with low pressure and should be removed without any residue. The applications of PSA are especially challenging in the medical field, where they are used for disease treatments on human skin. Their adhesion and detaching behavior has to be tested both in the short-term range as well as in the long-term range with respect to a given substrate.

The long-term behavior is often tested by shear tests where a static shear load is applied to an adhesive on a substrate, mostly a metal plate, and the time to the detaching is measured to affirm the sufficient cohesion. Peel tests determine the detaching force at angles of 90° or 180° for a constant peel-off velocity. In early tack testing performed with the rolling ball, the traveling distance of different sized stainless steel balls were obtained on faced up tapes [1]. Later developed methods recorded the magnitude of holding forces from freely turning smooth or toothed wheels, which rolled over adhesive-coated speed-controlled drums [1]. As an alternative, probe and loop tack testing evolved and were established as standardized methods for determination of a tack [2,3]. Here, the maximum forces were determined during retracting loops of adhesive tapes from stainless steel plates or stainless steel probes from a tape. Nowadays, the loop tack and the probe tack tests are widely used methods within the quality assurance and the development of the PSA [1,4,5].

The medication containing PSA controls the drug-release to the skin. According to medical regulations,[1,2] the probe tack tests must be performed for TTS, although they provide only the maximum detaching force without further information on the deformation dependent PSA behavior [2].

Several researchers tried to improve tack measurements by evaluating force-retraction displacement curves instead of only the maximum detaching force [6–14]. Then, effects of

a)Author to whom correspondence should be addressed; electronic mail: hausnerova@utb.cz

[1]Food and Drug Administration (FDA), Transdermal and topical delivery systems—Product development and quality considerations (2019), https://www.fda.gov/regulatory-information/search-fda-guidance-documents/transdermal-and-topical-delivery-systems-product-development-and-quality-considerations (accessed 18 February 2022).
[2]European Medicines Agency, Guideline on quality of transdermal patches (2015), https://www.ema.europa.eu (accessed 18 February 2022).

other test parameters such as retraction speed or dwell time could be investigated as well.

Furthermore, a cavity and a fibril generation during detaching were observed with optical methods [6,8–11]. Devices for improved tack measurements were laboratory designs, commercially available texture analyzers [13], or rheometers[3,4,5,6,7] using stiff metal substrates or glass slides during video monitoring. To the best of our knowledge, no study was found in which the tack measurements in terms of the force-retraction displacement curves were provided with the simultaneous video monitoring of the patches having a flexible backing layer. Therefore, the approach presented in this paper links mechanical retraction speed dependent tack behavior and video monitoring to gain deeper insights into deformation processes during PSA detaching.

As the probe tack originates from technical bonding purposes, it provides limited information about the short-term adhesion characterization of TTS during medical applications [15]. In this respect, the correlation of industry standard tests to viscoelastic properties represents a tool of relevant interest. The review of the fundamental findings in such correlations was provided by Chang [16]. In more recent literature studies, the attempt to relate viscoelastic moduli to adhesion properties (peel, tack, and shear resistance) of various PSA can still be found. As an example, Taghizadeh and Ghasemi [17] reported a strong dependence between peel strength and viscoelastic energy dissipation ($G''$) at higher frequency (100 Hz); the peel strength of samples increased with increased loss modulus. The tack values as well as shear resistance were related to storage modulus ($G'$) at frequencies of 1 and 0.1 Hz, respectively. While tack increased with decreasing $G'$, the shear resistance was related in the opposite way. TA Instruments[8] also proposed the viscoelastic criteria ($\tan\delta$, $G'$, $G''$) for a tack, shear resistance, peal strength, and cohesive as well as adhesive strengths.

Nevertheless, regardless of a possibility to separate bonding and debonding of PSA with viscoelastic frequency windows, the linking of material behavior from short amplitude oscillatory shear (SAOS) rheology to behavior during tests ending up in large deformations (peel and tack) remains a challenge. Currently, some effort (e.g., [18,19]) is also spent to relate extensional experiments to peel as it is a dominant mode of a PSA deformation during debonding, but regardless of comprehensive correlation of transient extensional viscosity to peel tests, Christensen and McKinley [19] did not arrive into a quantitative agreement of the measured and modeled values of peal forces (model based on both linear and nonlinear constitutive equations) without considering the strain-hardening behavior, which is another important factor even for shear strength testing [20].

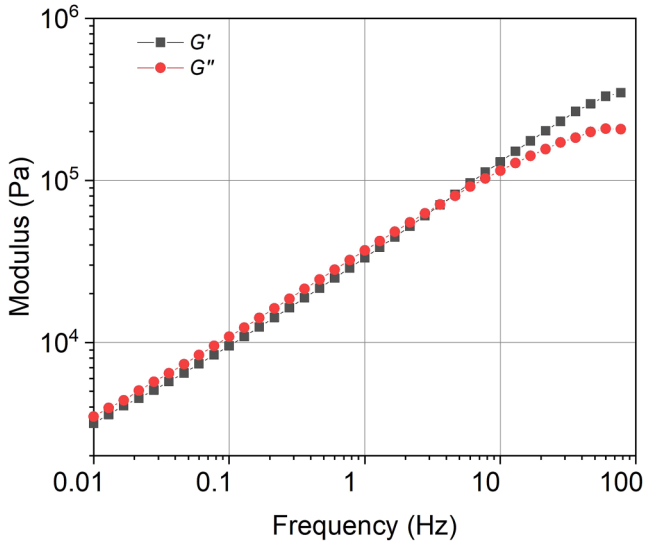


**FIG. 1.** Frequency dependent $G'$ and $G''$ curves of NAC-PSA from linear viscoelastic region at 30 °C with applied 1% strain amplitude.

Additionally, daily life motion causes skin strains up to 40%, which must be sustained by TTS for a complete application time [21–23]. Therefore, in our previous investigation [24], large amplitude oscillatory shear (LAOS) measurements were performed to investigate and to interpret the state of PSA during such high deformations.

The results of this research [24] clearly showed that standardized rheological measurements in the linear viscoelastic range are not relevant for medical applications, and straightforward relation of LAOS data to tack analysis is not available yet. In this paper, a new tack testing method, RheoTack, is presented as the first attempt to monitor PSA deformation performance at more relevant conditions than currently standardized, and further relate the obtained parameters to the data from LAOS rheological observations.

## II. EXPERIMENTAL

### A. Materials

TTS consisted of a backing layer and a silicone-based 7-4601 BIO PSA supplied by DuPont® and Dow Health Care Solutions®. It is a nonamine-compatible (NAC) PSA consisting of cross-linked polymer (50.9 vol. %) and resin components (49.1 vol. %).[9] The mean surface energy of the

[3]TA Instruments, Pressure-sensitive adhesive tack using the ARES rheometer (1999), http://www.tainstruments.com/pdf/literature/L2084_Tack_Testing_ARES.pdf (accessed 18 February 2022).

[4]Malvern Instruments, Application note: Assessing tackiness and adhesion using a pull away test on a rotational rheometer (2015), https://cdn.technologynetworks.com/TN/Resources/PDF/AN150527AssessingTackinessPullAway.pdf (accessed 18 February 2022).

[5]NETZSCH Gerätebau GmbH, Application note: Determination of pressure-sensitive tack and adhesion using axial measurements on a rotational rheometer—Blu-Tack® (2021), www.netzsch.com (accessed 18 February 2022).

[6]TA Instruments, Application note: Rheological analysis of tack (2021), http://www.tainstruments.com/pdf/literature/AAN018_V1_Analysis%20of%20tack.pdf (accessed 18 February 2022).

[7]Anton Paar, Application note: Combined rheological methods: From rheo-optics to magneto-rheology and beyond (2021), https://www.anton-paar.com (accessed 18 February 2022).

[8]TA Instruments, Characterization of pressure sensitive adhesives by rheology, https://www.tainstruments.com/pdf/literature/RH082.pdf (accessed 18 February 2022).

[9]DuPont, Product information: Liveo™ BIO-PSA 7-4601 standard silicone adhesives (2021), https://dupont.materialdatacenter.com/gb/products/pdf/SI/Liveo%E2%84%A2%20BIO-PSA%207-4601-gb.pdf (accessed 18 February 2022).

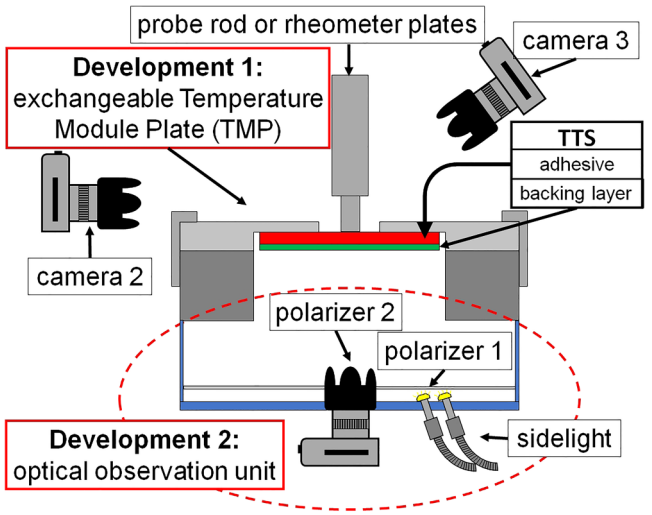


**FIG. 2.** Setup of the RheoTack experiment with upper rheometer plate as a probe rod, TMP for patch fixation substituting the bottom plate of the rheometer; observation unit for the RheoTack documentation from bottom (90°, camera 1), lateral (0°, camera 2), and top (45°, camera 3) implemented to the rheometer.

PSA was calculated from contact angle measurements (Surface Analyzer Kruss, Germany) with de-ionized water and ethanol at room temperature. The PSA films with a thickness of 150 $\mu$m ± 10% (thickness of commercial TTS) were manufactured using a coating box and finally laminated with the transparent backing layer consisting of polyester coated with ethylene-vinyl acetate (3M Scotchpak™ 9732). Oscillatory measurements on a rheometer (Haake MARS III, Thermo Fisher Scientific, Waltham, MA, USA) at a temperature of 30 °C within the linear viscoelastic region (strain amplitude of 1%) yielded the $G'$–$G''$ crossover point at a frequency of 4 Hz, Fig. 1, showing that PSA is operated in the gel region.

## B. Apparatus

As it can be operated both in compression and tension modes, the rheometer (Haake MARS III, Thermo Fisher Scientific, Waltham, MA, USA) was also used to perform the retraction rate dependent tack experiments. To allow for RheoTack experiments, it had to be supplemented by the following:

- **Sample holder**: The temperature module plate (TMP) with a diameter of 12 mm for the patch fixation substituted in the lower rheometer plate.
- **Video-monitoring system** consisting of 3 cameras allowing for the observation of the tack measurements from the bottom (camera 1 with angle 90°), the lateral (camera 2 with angle close to 0°), and the top (camera 3 with angle 45°) directions.
- **Illumination unit** underneath the TMP provides polarized lateral illumination; camera 1 (IC4203CU, Net, Finning, Germany) consisting of a magnifying lens (25 mm C-series, Edmund, Mainz, Germany) with a polarizer (Edmund, Mainz, Germany) can communicate with the rheometer software to time correlate pictures of the detaching processes to the corresponding force-retraction displacement-states; camera 2 (Canon EOS D60) and camera 3 (Canon EOS D800) both having focal lengths of 100 mm and are mounted above the TMP. The start of the measurement is marked with a laser flash. The experimental setup is shown in Fig. 2.
- **Exchangeable probe rod geometry:** different rheometric plates and other geometries can be mounted as an upper plate using an adapter; for RheoTack, a plate made of stainless steel (diameter of 8 mm with a roughness of 3025 ± 783 nm) is used.

## C. Execution of measurements

ASTM D2979-16 [2] recommends using a stainless steel rod of 5 mm diameter with a roughness of 250–500 nm, a sample holding ring providing a contact pressure of 9.79 kPa, a dwell time of 1 s, and a retraction speed of 10 mm/s. For RheoTack, an upper rheometer plate with a diameter of 8 mm was used as a probe rod due to its convenience for optical analysis. Surface roughness of the rod (3025 ± 783 nm) was in the range of values relevant for human skin. The plate having the smaller diameter (5 mm) was tested too, and no changes in the resulting force displacement curve shape due to the different rod to diameter ratio of the TMP was obtained. Then, the TTS samples with a diameter of 20 mm were attached to the TMP. The probe rod moved downward with a speed of 0.1 mm/s until reaching a compression force $\boldsymbol{F_I}$ of 0.2 N. This force was held for a dwell time $\boldsymbol{t_d} = 1$ s to provide an initial adhesion. The parameters $\boldsymbol{F_I}$ and $\boldsymbol{t_d}$ were adapted from ASTM D2979-16 [2] to ensure comparable states of the adhesion initiation. Although Tordjeman *et al.* [9] described increasing tack energies and tack forces with increasing PSA thickness, the PSA film thickness for the tests were chosen in the range of TTS patches (higher than recommended from the ASTM standard) to test the material at the practice-relevant conditions. Retraction speeds $v_{\text{retract}}$ of 0.01, 0.1, and 1 mm/s were chosen to investigate the viscoelastic tack behavior. Assuming homogeneous deformation of the 150 $\mu$m thick films, these retractions speeds correspond to the strain rates of 0.067, 0.67, and 6.7 l/s, which are within the time scales of application-related states during bonding and debonding [25].[10] In reality, the strain rates are less than one half as the backing layer is also shifted upward, Fig. 3. Retraction forces were measured at room temperature.

Simultaneously, video streams of three cameras were recorded. The zero displacement was determined by the displacement at which the stress changes from the compression to the tension. The RheoTack method provides the force-retraction displacement curves having a good reproducibility until reaching the maximum force $F_{\text{max}}$. Beyond $F_{\text{max}}$, the force exhibits a pronounced scatter.

[10]Dow Corning, Integrating rheological tools into the development and characterization of silicone adhesives (2021), https://citeseerx.ist.psu.edu/viewdoc/download?doi=10.1.1.580.4403&rep=rep1&type=pdf (accessed 18 February 2022).

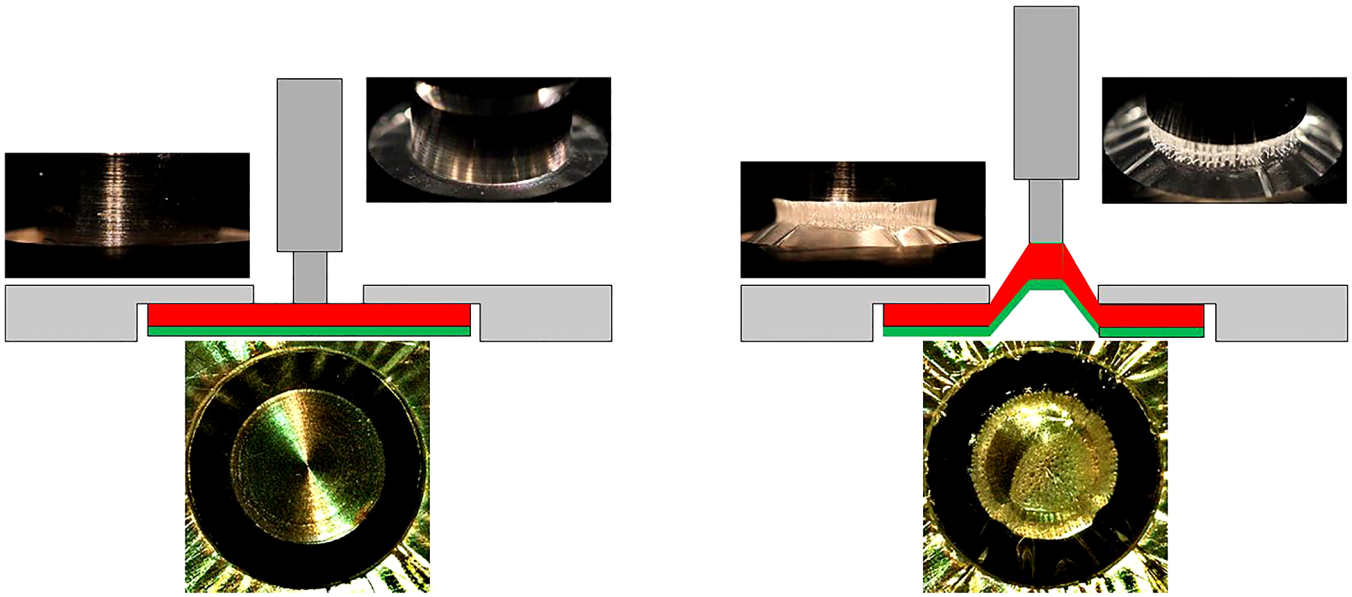

**FIG. 3.** Scheme of RheoTack analysis with upward shifting of the TTS and the formation of cavities and fibrils.

## III. RESULTS AND DISCUSSION

From the RheoTack experiments, two types of information can be extracted with respect to the detaching behavior—mechanical information in terms of force-retraction displacement curves and visual information in terms of deformation-induced structures of adhesives. The force-retraction displacement curve, Fig. 4, contains significantly more information about the detaching behavior than the single point measurement as the probe tack test according to ASTM D2979-16 [2].

Retraction speed dependent measurements can be performed with the retraction speeds ranging from 0.001 to 7 mm/min. The force displacement curve can be divided into the three phases—compression, stretching and fibrillation, and detaching—allowing for the evaluation of the following characteristic quantities:

- **sample stiffness** $\boldsymbol{S}$ as a slope at the displacement $h = 0$, when the compression turns to the tension,
- initiation force of cavity and/or fibril formation $F_{\text{start fib}}$ and corresponding displacement $h_{\text{start fib}}$,
- activation energy of cavity and/or fibril formation $E_{\text{start fib}}$,
- maximum force $F_{\text{max}}$ and corresponding displacement $h_{\text{max}}$, and
- **adhesion energy** $\boldsymbol{E_{\text{adh}}}$ as the integral of the force displacement curve until the complete loss of adhesion.

As the detaching process is monitored with three cameras from the bottom (90°), lateral (0°), and top (45°), macroscopically visible structural changes can be linked to the three phases of the force-retraction displacement curves and the characteristic quantities. During the compression phase, the adhesion between the PSA and the probe rod is established due to the chosen initial force and dwell time. This adhesion or wetting process depends on several factors as surface energies and polarity of a substrate and an adhesive as well as temperature. Only high substrate and low adhesive surface energies will lead to a good wettability of a substrate [26]. In the case of the tested PSA, the free surface energy 15.6 mN/m was obtained, while the stainless steel features values around 50 mN/m [27]. From this point, a good wettability can be expected. In addition, the adhesion of PSA depends on a dwell time and a compression force [28,29], which are governed by viscoelastic properties of the PSA [1,8]. When the retraction starts, the load case turns from the compression to the tension during which the sample is deformed in an almost homogeneous manner. The slope of the force displacement curve at the displacement $h = 0$ represents a measure of the retraction speed dependent stiffness $S$ of the PSA,

$$S = \lim_{h \to 0} \frac{\partial F(h)}{\partial h}. \tag{1}$$

If the force exceeds $F_{\text{start fib}}$, the deformation behavior becomes inhomogeneous attained with the visible stretching marks on the TTS in the gap. Further tensile deformation generates first cavities and fibrils along the edge of the probe rod if $F_{\text{start fib}}$ is exceeded, Fig. 4. Then, the cavity and fibril formation is directed toward the middle. With ongoing retraction displacement, the PSA loses adhesion to the probe rod over a certain part of the contact area indicated by a "bubble" formation. As the oriented fibrils can transfer higher loads, the backing layer is further stretched and it steepens up. This leads to the further fibril formation in the remaining homogeneously deformed regions, which still have the contact to the rod. The "bubble" formation may provide the material for the further fibril formation. When reaching $\boldsymbol{F_{\text{max}}}$, detaching begins either by fibril breakage or adhesion failure to the probe. This is indicated by a significantly increased scatter of the force due to the arbitrary nature of the fibrils breakage.

Figure 5 shows the effects of the retraction speed on the force-retraction displacement curves. At the beginning, the increase in force seems to be similar for all retraction speeds.

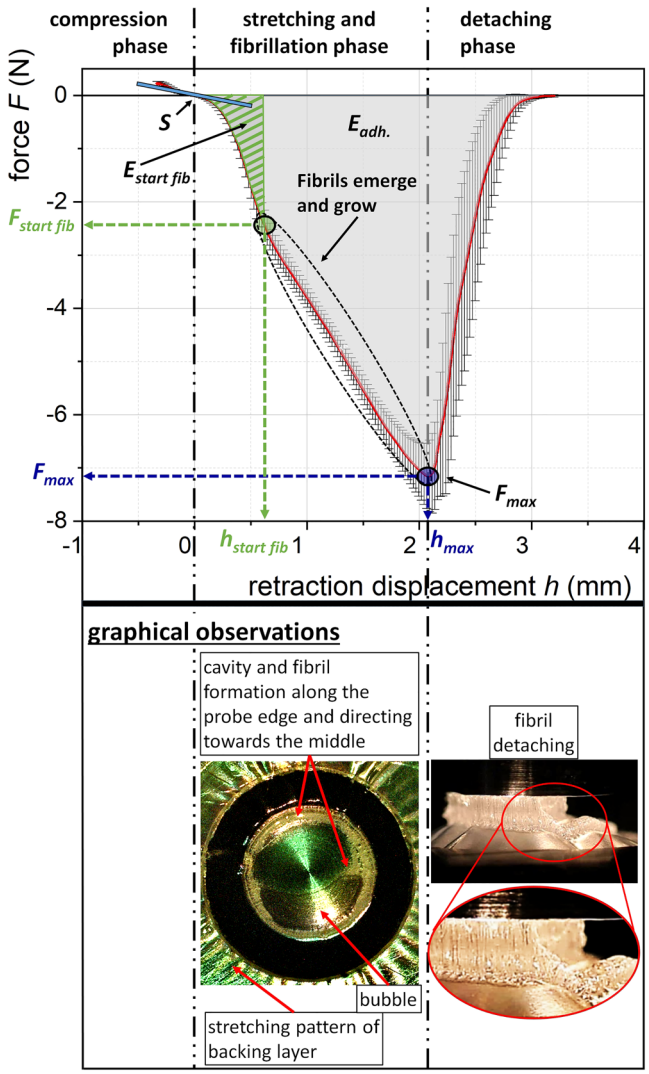


**FIG. 4.** RheoTack analysis: force-retraction displacement curve with deformation phases and characteristic quantities $S$, $F_{\text{start fib}}$, $h_{\text{start fib}}$, $F_{\max}$, $h_{\max}$, $E_{\text{start fib}}$ and $E_{\text{adh}}$, and corresponding structures at $F_{\text{start fib}}$ and $F_{\max}$ (TTS with a NAC-PSA).

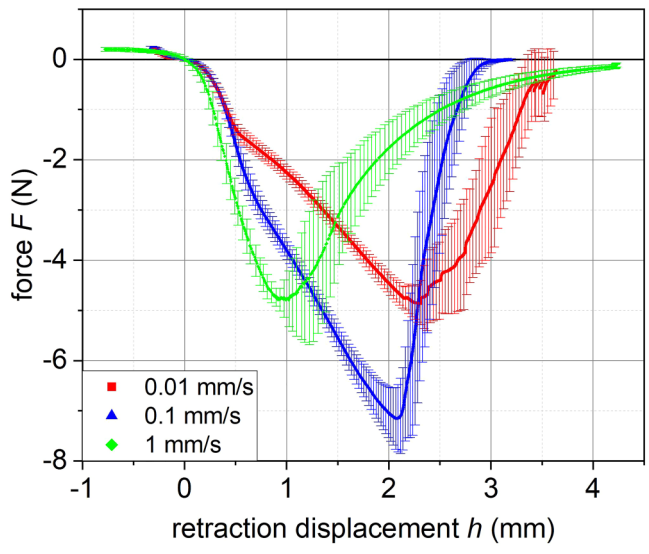


**FIG. 5.** Mean force-retraction displacement curves at retraction speeds of 0.01, 0.1, and 1 mm/s obtained for five different TTS samples.

After reaching $h_{\text{start fib}}$, the increase in force is reduced due to the fibrils formation and the corresponding PSA flow. With increasing retraction speed, the PSA stiffness $S$ is increased due to the viscoelastic behavior, and the fibrils formation requires higher activation energies $E_{\text{start.fib}}$. Both quantities increase by a factor of 3 when the retraction speed is increased from 0.01 to 1 mm/s, Table I. Interestingly, the displacement $h_{\text{start fib}}$ hardly depends on the retraction speed indicating that the start of fibrils formation is a strain triggered parameter. At the retraction speed of 1 mm/s, fibrils formation is initiated, but the fibrils have no sufficient time to generate enough material flow due to the more solid statelike behavior. The fibrils break faster at higher retraction speeds indicated by the decrease of $F_{\max}$ and $h_{\max}$. The adhesion energy $E_{\text{adh}}$ seems to be similar for 0.01 and 0.1 mm/s indicating rather constant activation energy in the liquid phase, which is decreased if the PSA behaves stiffer at 1 mm/s. These findings are in contrast to the results of Lakrout *et al.* [10] and Kim and Mizumachi [30], who found increasing $F_{\max}$ and $E_{\text{adh}}$ with retraction speeds for an acrylic PSA.

All force-retraction displacement curves in Fig. 5 show little force scatter before reaching $F_{\max}$ for five different TTS samples. This means that deformation takes place in a rather uniform manner by the homogeneous tensile deformation of the PSA followed by the continuous stretching of the fibrils. For the deformations beyond $F_{\max}$, the fibrils start to break, which is an arbitrary failure and a detaching process leading to a significant scatter in the force signal indicated by three to four times larger error bars of the average curves.

If the defined deformation states of the force-retraction displacement curves for the retraction rates of 0.01, 0.1, and 1 mm/s are linked to the corresponding deformation structures monitored by the three cameras, one gains deeper insights into the occurring deformation processes, Figs. 6–8. The following deformation processes can be identified. First, the deformation behavior seems to be homogeneous at the beginning of the retraction (deformation state "1"). Second, if the force exceeds $F_{\text{start fib}}$, the cavity and/or the fibril formation is/are initiated along the circumference of the probe rod (deformation state "2"). This is associated by a "bubble" formation (deformation states "2" and "3") indicating the sudden loss of adhesion over a certain part of the cross section. Camera 3 shows smooth areas without any fibrillated structure, deformation state "6." In the deformation range between $h_{\text{start fib}}$ and $h_{\max}$, the fibrils are continuously stretched and the process of fibril formation moves toward the center of the probe rod. At the deformation states "3" and "4," camera 2 shows differently strained fibrils along the edge of the probe rod. This means that after establishing a certain tensile stress in the TTS of the gap, further deformation is attributed to the fibril stretching and formation, camera 2 states "3, 4, and 5" in Fig. 6. Third, if the force reaches $F_{\max}$, the strength of the fibrils at the edge of the probe rod is exceeded and they either break (cohesive failure) or detach from the probe rod (adhesive failure), deformation states "5" and "6." A sudden force reduction is observed due to the simultaneous failure of highly loaded fibrils. Then, a lower force level is established on which the remaining so far less loaded fibrils are deformed until failure. A stepwise

**TABLE I.** Retraction speed dependent characteristic quantities of NAC-PSA.

| $v_{retract}$ (mm/s) | $S$ (N/mm) | $F_{start\ fib}$ (N) | $h_{start\ fib}$ (mm) | $E_{adh.fib}$ (mJ) | $F_{max}$ (N) | $h_{max}$ (mm) | $E_{adh.}$ (mJ) |
|---|---|---|---|---|---|---|---|
| 0.01 | 0.18 ± 0.05 | −1.5 ± 0.2 | 0.50 ± 0.04 | 0.27 ± 0.04 | −5.0 ± 0.3 | 2.4 ± 0.3 | 9.3 ± 1.1 |
| 0.1 | 0.39 ± 0.10 | −2.6 ± 0.2 | 0.65 ± 0.07 | 0.57 ± 0.11 | −7.3 ± 0.7 | 2.1 ± 0.1 | 10.2 ± 1.2 |
| 1 | 1.07 ± 0.06 | −3.5 ± 0.5 | 0.59 ± 0.06 | 0.82 ± 0.23 | −5.3 ± 0.7 | 1.0 ± 0.1 | 7.3 ± 1.2 |

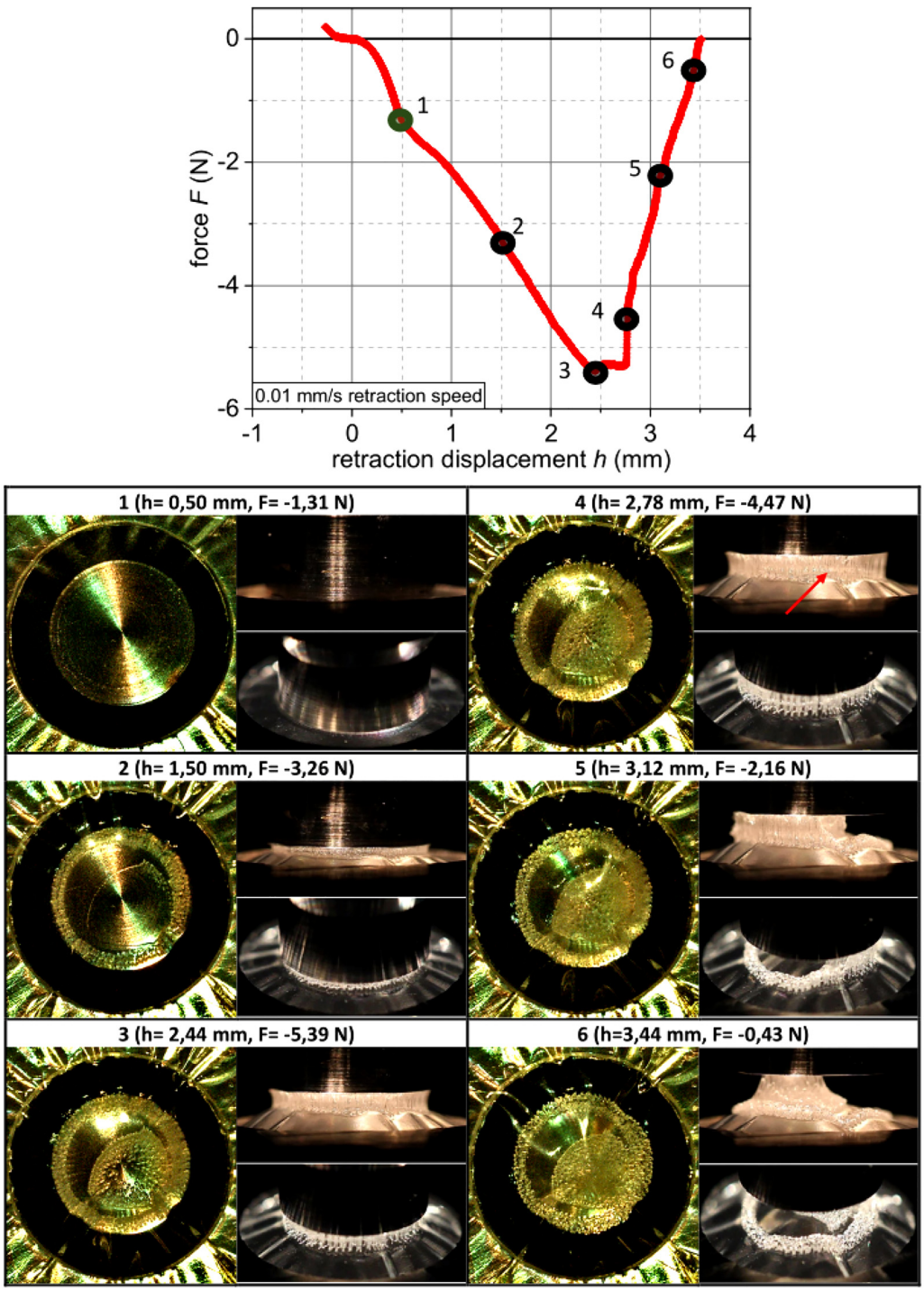


**FIG. 6.** Force-retraction displacement curves with six indicated deformation states and the corresponding deformation structures observed with camera 1 under the probe rod in 90° (left), camera 2 parallel to the TMP under 0° (top right), and camera 3 under 45° (bottom right) for a TTS with NAC-PSA at retraction speed of 0.01 mm/s.

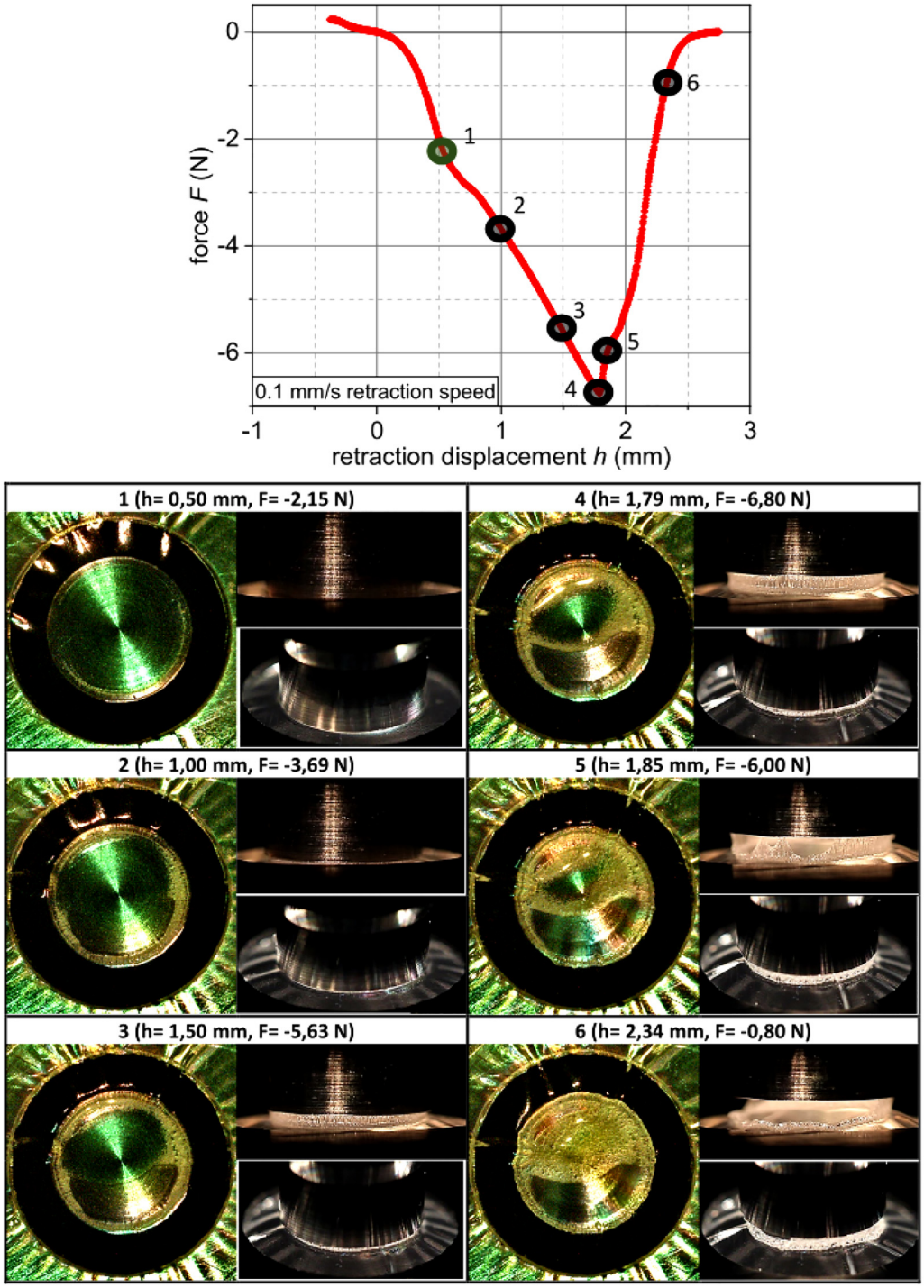


**FIG. 7.** Force-retraction displacement curves with six indicated deformation states and the corresponding deformation structures observed with camera 1 under the probe rod in 90° (left), camera 2 parallel to the TMP under 0° (top right), and camera 3 under 45° (bottom right) for a TTS with NAC-PSA at retraction speed of 0.1 mm/s.

force decrease is observed as the fracture and adhesion failure of fibrils are arbitrary processes due to variations of diameter, contact area, and strength. Finally, the PSA loses the contact to the probe rod completely. If the "bubble" formation occurs, the contact areas do not show any deformed structure, camera 3, deformation state "6." This indicates the instantaneous loss of the adhesion.

Maurer [6] and Brown and Creton [14] detected first cavities and fibrils near the maximum force $F_{max}$ for different PSA using a stiff glass substrate. This demonstrates that the substrate affects significantly the adhesion and detaching behavior as the use of the flexible backing layer as the substrate leads to the formation of cavities and fibrils already at the $F_{start\ fib}$ forces being a factor of 3 smaller than $F_{max}$.

With increasing retraction speed, the distinction of the cavities becomes less clear. The decreasing cavity size was found also by Lakrout *et al.* [10] for acrylates, Nase [8] for polydimethylsiloxanes, or Brown *et al.* [11] for

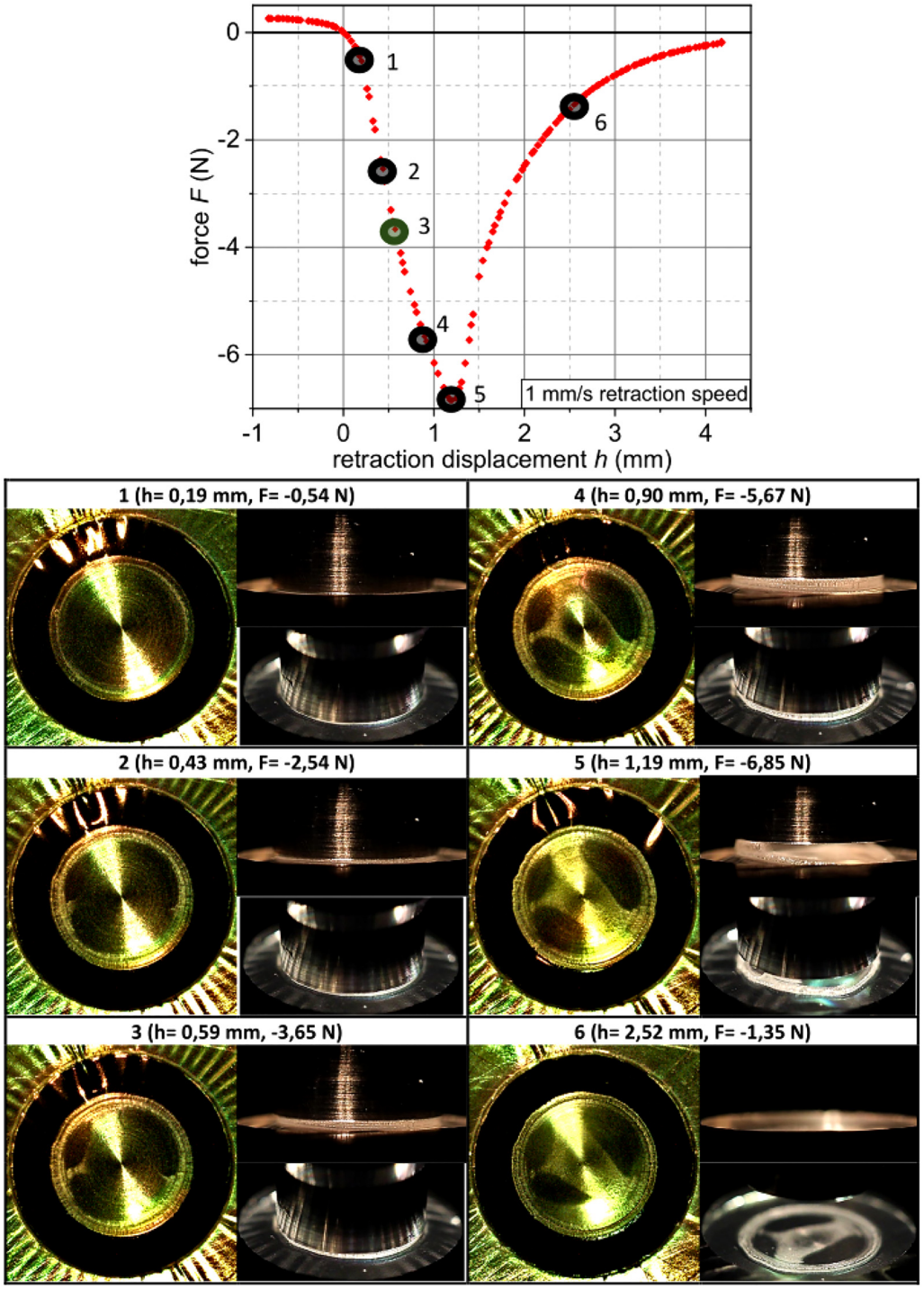


**FIG. 8.** Force-retraction displacement curves with six indicated deformation states and the corresponding deformation structures observed with camera 1 under the probe rod in 90° (left), camera 2 parallel to the TMP under 0° (top right), and camera 3 under 45° (bottom right) for a TTS with NAC-PSA at retraction speed of 1 mm/s.

styrene-isoprene-styrene. At retraction speeds of 0.01 and 0.1 mm/s, only one bubble is formed, while for 1 mm/s, three bubbles occurred. This may indicate that at small retraction speeds, the bubble formation starts at a single weak point in the interface between the PSA and the probe rod. This weak point is created by the first cavity and the fibril formation as these form channels for the inflowing air to fill the gap between PSA and the probe rod. Lakrout *et al.* [10] reported similar observations and explained them as a quick pressure compensation linked to a slope decrease of a force-retraction displacement curve.

The videos in the supplementary material visualize the retraction speed dependent deformation behavior of TTS during the RheoTack experiments and correlates it with the corresponding force-retraction displacement curves. The visualizations show that the first detaching processes (marked by red circles) are seen by camera 2 at 2 min 20 s (0.01 mm/s-video [31]) and 21 s (0.1 mm/s-video [31]). The rupture of

the first fibril—the arrow in Fig. 6, deformation state "4"—reduces locally the stress in the TTS of the gap, and thus its inclination. The 0.01 and 0.1 mm/s videos [31] show the corresponding beginning of the downward movement of the TTS, which leads to the break or the detaching of the fibrils until new equilibrium is established. At the retraction speed of 1 mm/s [31], the break of fibrils is so fast that it cannot be resolved in time with the cameras, but similar deformation behavior can be assumed from the force-retraction displacement curves.

The fibril formation starts at the circumference of the probe rod forming the fibrillar ring. Then, it moves around the bubble toward the center of the remaining adhesive contact area until complete fibril formation is achieved. Finally, a stepwise detaching of the PSA from the probe rod occurs until complete detaching. For the retraction speed of 1 mm/s, the fibrillar ring is formed, but there is not enough time to fibrillate the remaining contact area completely. The structure of the fracture surface exhibits areas, which fail rather in a brittle manner (as also reported by Lakrout *et al.* [10]).

As can be clearly seen, during tack testing, different states of material deformation occur. As patch stiffness is determined by the slope at zero crossing of force, it can be related to the complex modulus $G^*$ within the linear viscoelastic region. The fibrillation, however, features larger deformations beyond the SAOS testing. Thus, the description of TTS behavior should be related rather to the behavior at large deformations quantitatively determined by LAOS measurements. The strain rate dependent $F_{\text{start fib}}$ showed a logarithmic dependency. The same trend is found for the frequency dependent strain amplitude $\gamma_{0C}$ representing the limit of the linear viscoelastic region [24]. Thus, in the following research, the results obtained with RheoTack will be derived for the set of PSA resins and related to their LAOS characteristics.

## IV. CONCLUSION

In this study, a new method to characterize the adhesion and detaching behavior of medical adhesives was presented. RheoTack analysis can be installed in all commercially available rotational rheometers, which allow for measuring normal forces. Thus, force-retraction displacement curves can be measured for different retraction speeds, compression forces, dwell times, and geometries of probe rods. In particular, RheoTack provides insight into the adhesion and detaching behavior of PSA applied on human skin. With the proposed TMP sample holder, adhesives with flexible backing layers can be easily investigated. Although the tack tests according to ASTM D2979 represent the single point measurement, the force-retraction displacement curves of the RheoTack allow us to determine the stiffness, start and activation energy of fibril formation, strength (maximum load), and start of a PSA failure. The implementation of three cameras provides the qualitative observation of the deformation-induced structural changes of PSA such as cavity and fibril formation, bubble formation (loss of adhesion between a PSA and a probe rod), or failure due to break and detaching of fibrils. This can be linked to the load conditions of the corresponding force-retraction displacement curve. The investigation of the adhesion and detaching behavior of the NAC PSA shows that both characteristic properties and the deformation structure depend strongly on the retraction speed. Thus, RheoTack analysis represents a powerful tool in the development of tailored PSA and their quality control.

## ACKNOWLEDGMENTS

This study was supported by the German Ministry of Education and Research (Grant No. 03FH039PX5). B.H. acknowledges the Ministry of Education, Youth and Sports of the Czech Republic - DKRVO (No. RP/CPS/2022/003). M.M. also acknowledges the Graduate Institute Bonn-Rhein-Sieg University of Applied Sciences for supporting this work by granting a scholarship. The R&D unit of Thermo Fisher Scientific in Karslruhe is specially acknowledged.

## AUTHOR DECLARATIONS

### Conflicts of Interest

The authors have no conflicts to disclose.

## DATA AVAILABILITY

The datasets generated during and/or analyzed during the current study are available in the Zenodo open repository maintained by https://doi.org/10.5281/zenodo.5603015, Ref. 32.

## REFERENCES

[1] Hammond, F. H. J., and C. Kendall, Tack, in *Handbook of Pressure Sensitive Adhesive Technology*, edited by D. Satas (Springer Science +Business Media, New York, 1989), Vol. 2.

[2] American Society for Testing and Materials (ASTM), *Standard Test Method for Pressure-Sensitive Tack of Adhesive Using an Inverted Probe Machine—ASTM D2979* (ASTM International, West Conshohocken, PA, 2016), Vol. 15.10 (this method was withdrawn by the jurisdiction of committee in April 2019 without replacement due to a limited use by industry).

[3] CEN European Committee for Standardization, *Adhesives for Paper and Board, Packaging and Disposable Sanitary Products—Tack Measurement for Pressure Sensitive Adhesives—Determination of Loop Tack (DIN EN 1719:1998)* (Beuth Verlag GmbH, Berlin, 1998), Vol. 1791998-11.

[4] Wokovich, A. M., S. Prodduturi, W. H. Doub, A. S. Hussain, and L. F. Buhse, "Transdermal drug delivery system (TDDS) adhesion as a critical safety, efficacy and quality attribute," Eur. J. Pharm. Biopharm. **64**, 1–8 (2006).

[5] Ho, K., and K. Dodou, "Rheological studies on pressure-sensitive silicone adhesives and drug-in-adhesive layers as a means to characterise adhesive performance," Int. J. Pharm. **333**, 24–33 (2007).

[6] Maurer, E., Strukturuntersuchungen an Haftklebstoffen beim mechanischen tack-test auf makroskopischer und mikroskopischer Längenskala, Dissertation - monograph, University of Munich, 2005.

[7] Maurer, E., S. Loi, D. Wulff, N. Willenbacher, and P. Müller-Buschbaum, "Microscopic structure in pressure sensitive

adhesives: An ultrasmall angle X-ray study," Physica B **357**, 144–147 (2005).

[8] Nase, J., Debonding of viscoelastic materials: From a viscous liquid to a soft elastic solid, Dissertation - monograph, Saarland University, 2009.

[9] Tordjeman, P., E. Papon, and J.-J. Villenave, "Tack properties of pressure-sensitive adhesives," J. Polym. Sci. Pol. Phys. **38**, 1201–1208 (2000).

[10] Lakrout, H., P. Sergot, and C. Creton, "Direct observation of cavitation and fibrillation in a probe tack experiment on model acrylic pressure-sensitive-adhesives," J. Adhesion **69**, 307–359 (1999).

[11] Brown, K., J. C. Hooker, and C. Creton, "Micromechanisms of tack of soft adhesives based on styrenic block copolymers," Macromol. Mater. Eng. **287**, 163–179 (2002).

[12] Heddleson, S. S., D. D. Hamann, and D. R. Lineback, "The Dahlquist Criterion: Applicability of a rheological criterion to the loss of pressure-sensitive tack in flour-water dough," Cereal Chem. **70**, 744–748 (1993).

[13] Boris, E. G., E. V. Bermesheva, G. A. Shadryuk, and M. M. Feldstein, "Effect of temperature on probe tack adhesion: Extension of the Dahlquist criterion of tack," J. Adhesion **87**, 111–138 (2011).

[14] Brown, K. R., and C. Creton, "Nucleation and growth of cavities in soft viscoelastic layers under tensile stress," Eur. Phys. J. E **9**, 35–40 (2002).

[15] Venkatraman, S., and R. Gale, "Skin adhesives and skin adhesion: 1. Transdermal drug delivery system," Biomaterials **19**, 1119–1136 (1998).

[16] Chang, E. P., "Viscoelastic properties of pressure-sensitive adhesives," J. Adhesion **60**, 233–248 (1997).

[17] Taghizadeh, S. M., and D. Ghasemi, "Rheological and adhesion properties of acrylic pressure-sensitive adhesives," J. Appl. Polym. Sci. **120**, 411–418 (2011).

[18] Creton, C., and M. Ciccotti, "Fracture and adhesion of soft materials: a review," Rep. Prog. Phys. **79**, 046601 (2016).

[19] Christensen, S. F., and G. H. McKinley, "Rheological modelling of the peeling of pressure-sensitive adhesives and other elastomers," Int. J. Adhes. Adhes. **18**, 333–343 (1998).

[20] Lui, Z., H. Minsky, C. Creton, M. Ciccotti, and C. Y. Hui, "Mechanics of zero degree peel test on a tape—Effects of large deformation, material nonlinearity, and finite bond length," Extreme Mech. Lett. **32**, 100518 (2019).

[21] Wessendorf, A. M., and D. J. Newman, "Dynamic understanding of human-skin movement and strain-field analysis," IEEE Trans. Biomed. Eng. **59**, 3432–3438 (2012).

[22] Maiti, R., L. C. Gerhardt, Z. S. Lee, R. A. Byers, D. Woods, J. A. Sanz-Herrera, S. E. Franklin, R. Lewis, S. J. Matcher, and M. J. Carré, "*In vivo* measurement of skin surface strain and sub-surface layer deformation induced by natural tissue stretching," J. Mech. Behav. Biomed. **62**, 556–569 (2016).

[23] Ge, W., A. Sfara, and B. Hians, "Skin deformation during shoulder movements and upper extremity activities," Clin. Biomech. **47**, 1–6 (2017).

[24] Meurer, M., R. Kádár, E. Ramakers-van Dorp, B. Möginger, and B. Hausnerova, "Nonlinear oscillatory shear tests of pressure-sensitive adhesives (PSAs) designed for transdermal therapeutic systems (TTS)," Rheol. Acta **60**, 553–570 (2021).

[25] Michaelis, M., Characterization of pressure sensitive adhesive systems for transdermal patches, Dissertation - monograph, University of Hamburg, 2015.

[26] Packham, D. E., "Surface energy, surface topography and adhesion," Int. J. Adhes. Adhes. **23**, 437–448 (2003).

[27] Tang, S., O. J. Kwon, N. Lu, and H. S. Choi, "Surface free energy changes of stainless steel after one atmospheric pressure plasma treatment," Korean J. Chem. Eng. **21**, 1218–1223 (2004).

[28] Chatti, S., S. Laperrièr, G. Reinhart, and T. Tolio, *Bonding in The International Academy for Production Engineering, CIRP Encyclopedia of Production Engineering* (Springer, Berlin, 2014), Vol. 2.

[29] da Silva, L. F. M., A. Öchsner, and R. D. Adams, *Handbook of Adhesion Technology* (Springer, Berlin, 2011), Vol. 2.

[30] Kim, H. J., and H. Mizumachi, "Miscibility and probe tack of acrylic pressure sensitive adhesives—Acrylic copolymer/tackifier resin systems," J. Adhesion **49**, 113–132 (1995).

[31] See the supplementary material at https://www.scitation.org/doi/suppl/10.1122/8.0000405 for the complete rate dependent analysis of TTS using RheoTack; NAC_P8_150$\mu$m_0.01mm_s_video; NAC_P8_150$\mu$m_0.1mm_s_video; and NAC_P8_150$\mu$m_1mm_s_video.

[32] M. Meurer (2021). "RheoTack – A new method to investigate the rate dependent viscoelastic detaching behavior of pressure sensitive adhesives (PSA)," Zenodo.